nature materials

ARTICLES

PUBLISHED ONLINE: 26 SEPTEMBER 2016 | DOI: 10.1038/NMAT4757

Generation of subnanometric platinum with high stability during transformation of a 2D zeolite into 3D

Lichen Liu[1], Urbano Díaz[1], Raul Arenal[2,3], Giovanni Agostini[4], Patricia Concepción[1] and Avelino Corma[1,5]*

Single metal atoms and metal clusters have attracted much attention thanks to their advantageous capabilities as heterogeneous catalysts. However, the generation of stable single atoms and clusters on a solid support is still challenging. Herein, we report a new strategy for the generation of single Pt atoms and Pt clusters with exceptionally high thermal stability, formed within purely siliceous MCM-22 during the growth of a two-dimensional zeolite into three dimensions. These subnanometric Pt species are stabilized by MCM-22, even after treatment in air up to 540 °C. Furthermore, these stable Pt species confined within internal framework cavities show size-selective catalysis for the hydrogenation of alkenes. High-temperature oxidation–reduction treatments result in the growth of encapsulated Pt species to small nanoparticles in the approximate size range of 1 to 2 nm. The stability and catalytic activity of encapsulated Pt species is also reflected in the dehydrogenation of propane to propylene.

The unique catalytic properties of metal clusters have attracted great attention because they have a behaviour that is distinct from metal nanoparticles (NPs) and mononuclear metal compounds[1,2]. However, the stability of metal clusters can be a limitation for their applications in heterogeneous catalysis at higher temperatures. Loading atomically dispersed metal species on solid supports can be a method to improve their stability[3,4]. In this respect, because of their high thermal stability and confinement effects, zeolite materials appear as promising supports for preparing supported metal clusters[5]. By conventional methods (such as wet impregnation and ion exchange), the location of metal species cannot always be controlled, and metal NPs will usually be formed after the post-treatment. Moreover, during the reaction or during some harsh thermal treatments, active species on the external surface can aggregate to form large NPs (>5 nm), resulting in a decrease of catalytic activity[6–9].

Recently, Iglesia *et al.* have developed a method to encapsulate small metal NPs into microporous cavities during the synthesis of different zeolitic materials. Different types of metal NPs, with sizes in the approximate range of 1 to 2 nm, were encapsulated into zeolites such as Sodalite (SOD), Analcime (ANA) and Gismondine (GIS)[10,11]. This method has been used, so far, for the synthesis of Al-containing zeolites, and the metal nanoparticles encapsulated in those zeolites are resistant to sintering[12]. Nevertheless, in some cases, the introduction of Al into the zeolites may restrict the reaction scope of these materials because of the acidity associated with the presence of Al sites. Gates *et al.* have prepared single metal atoms and metal clusters (below 1 nm) confined in zeolites and performed excellent detailed characterizations on the location and atomic structure of these metal species[13,14]. In this case, metal clusters with identified atomicity can be anchored into the pores of pure-silica zeolites, and the stability of metal clusters obtained by thermal decomposition of the metal precursor (for example, organometallic compounds) could be an issue. In some cases, they may agglomerate even at room temperature under the ambient environment. Therefore, developing a facile and sustainable method for incorporating metal clusters in high-silica zeolites with high thermal stability is still a challenge.

In this work, we present a new strategy for the preparation of zeolite-confined subnanometric Pt species (single Pt atoms and Pt clusters) catalysts with high stability during transformation of a two-dimensional (2D) into three-dimensional (3D) zeolite. As the starting material, we choose a pure siliceous layered precursor of MCM-22 (MWW-type zeolite)[15] with the idea that, during the condensation of the layered zeolite precursor, the hemi-cages (cups) and cages—with internal dimensions of ∼0.7 and ∼0.7 × 1.8 nm, respectively—would entrap the subnanometric Pt species. The resultant material will be named as Pt@MCM-22. In this way, Pt individual atoms and Pt clusters will be incorporated into the cups and cages of MCM-22 zeolite. It will be shown that subnanometric Pt species in the cavities can differentiate reactants by size and show exceptional high thermal stability and better catalytic activity.

Structural characterization

The preparation process of Pt@MCM-22 is schematized in Fig. 1. To incorporate subnanometric Pt species into MCM-22, purely siliceous MWW precursor (namely ITQ-1) was first synthesized[16]. Subnanometric Pt species were prepared using dimethylformamide (DMF) as a weak reduction and capping agent[17,18]. The fluorescence emission spectrum and picture of the DMF solution containing subnanometric Pt species are shown in Supplementary Fig. 1. The incorporation of subnanometric Pt species was carried out during the swelling process of the lamellar zeolitic precursor (MWW(P)), which can be monitored by X-ray diffraction

[1]Instituto de Tecnología Química, Universitat Politècnica de València-Consejo Superior de Investigaciones Científicas (UPV-CSIC), Av. de los Naranjos s/n, 46022 Valencia, Spain. [2]Laboratorio de Microscopias Avanzadas, Instituto de Nanociencia de Aragon, Universidad de Zaragoza, Mariano Esquillor Edificio I+D, 50018 Zaragoza, Spain. [3]ARAID Foundation, 50018 Zaragoza, Spain. [4]European Synchrotron Radiation Facility, 6 rue Jules Horowitz, Grenoble, BP 156, F-38042, France. [5]King Fahd University of Petroleum and Minerals, PO Box 989, Dhahran 31261, Saudi Arabia. *e-mail: acorma@itq.upv.es

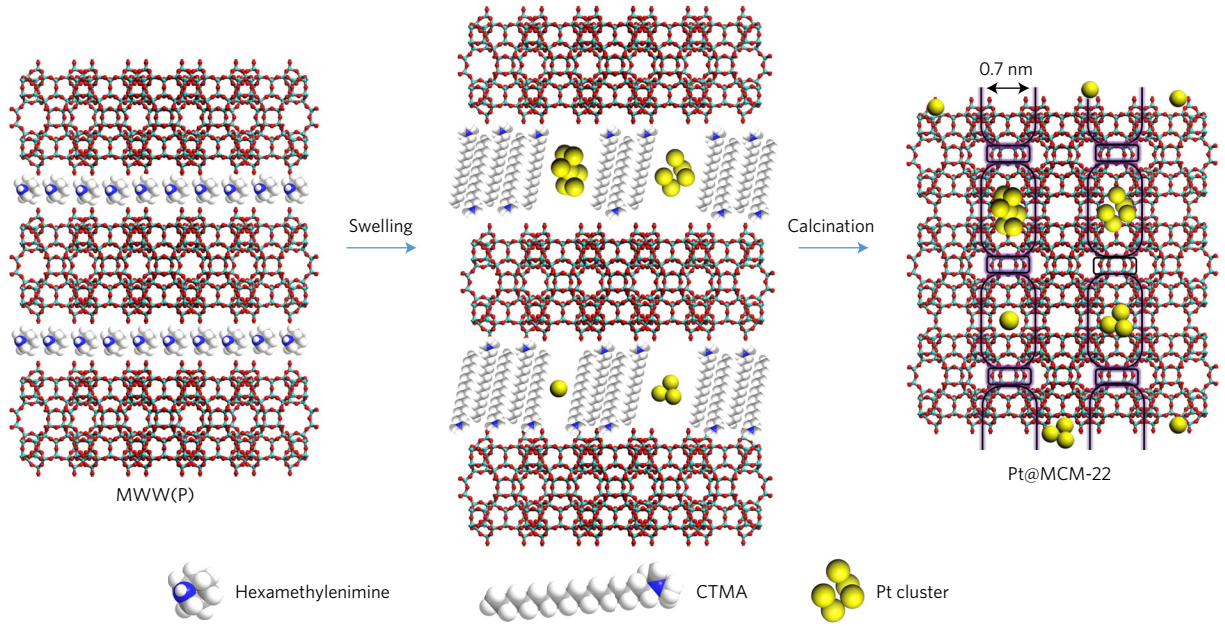

Figure 1 | Illustration of the preparation of Pt@MCM-22. During the swelling process of layered MWW zeolitic precursors (MWW(P)), a solution containing subnanometric Pt species is added. MWW layers are expanded by the surfactant (hexadecyltrimethylammonium, $CTMA^+OH^-$) and subnanometric Pt species are also incorporated into the internal channels between individual MWW layers. Removing the organic agents will lead to the formation of 3D Pt@MCM-22, in which subnanometric Pt species are confined in the external cups on the surface or encapsulated in the supercages of MCM-22.

(see Supplementary Fig. 2). After the swelling process, subnanometric Pt species as well as the surfactant molecules were located between the layers. Then, the organic surfactant was removed by calcination in air at 540 °C, leading to the formation of Pt atoms and clusters encapsulated by the supercages of 3D MCM-22, giving the final Pt@MCM-22 sample (the loading amount of Pt is 0.11 wt%, measured by inductively coupled plasma spectrometry (ICP)). As well as full encapsulation, Pt species could also be confined in the cups located at the external surface of the MWW crystallites.

The structures of as-prepared Pt@MCM-22 were characterized by transmission electron microscopy (TEM) and high-angle annular dark-field detector high-resolution scanning TEM imaging (HAADF-HRSTEM imaging). As shown in Fig. 2a, only MCM-22 crystallites can be seen in the TEM image. The hexagonal structure of MCM-22 is preserved after the incorporation of Pt species, as confirmed by the fast Fourier transform (FFT) and powder X-ray diffraction (XRD) patterns (Supplementary Fig. 3). In the STEM images (Fig. 2b), the 12 member-ring (MR) sub-units of the external cups in MCM-22, with diameters of approximately 0.7 nm, can be clearly seen from the view of the *c*-axis. Indeed, this imaging technique is chemical sensitive because it provides Z (atomic number)-contrast between heavy Pt atoms (bright features) and MCM-22 zeolite composed of light atoms[19]. The contrast for single Pt atoms has been analysed on the basis of the intensity profiles, as shown in Fig. 2e,f. The good dispersion of subnanometric Pt species is confirmed in additional STEM images (see Supplementary Figs 4 and 5). Furthermore, Pt clusters and individual Pt atoms with fine dispersion can be distinguished clearly in the HAADF-HRSTEM images (Fig. 2c,d). Further intensity profiles of different types of Pt species can be found in the Supplementary Information (see Supplementary Figs 6 and 7)[20]. It is worth mentioning that the intensity differences of the bright dots displayed in the HAADF-HRSTEM images maybe due to the focus conditions of the electron beam on the Pt atoms/clusters (or equivalently to the location of these atoms within the zeolite crystallites). For instance, Fig. 2e (area #2) and Supplementary Fig. 6 (area #3) clearly illustrate how the intensity of the dots corresponding to two neighbouring atoms is slightly different, indicating their different location in the MCM-22 crystallites. To better understand these findings, we have carried out HAADF-HRSTEM image simulations (see Supplementary Fig. 8). The simulation results confirm the interpretation of the experimental HRSTEM images, which correspond to individual Pt atoms and Pt clusters incorporated in MCM-22. Even though it is difficult to obtain the exact location of Pt species, some important information can still be obtained based on the HRSTEM images. As shown in Supplementary Figs 9 and 10, Pt single atoms and small clusters appear to be confined in the cups and at the connecting walls between the cups, while some Pt clusters could also be encapsulated in the supercages in MCM-22 (as illustrated in Fig. 2g). Meantime, there are also some atomically dispersed Pt species anchored on the framework of MCM-22. Since the internal dimensions of the supercages are 0.7 × 1.8 nm, 10–13 Pt atoms can be contained, considering their three-dimensional structures (a schematic illustration of a Pt_5 cluster confined in supercages of MCM-22 is shown in Fig. 2h)[21]. We could find only a few large Pt clusters (about 0.7–1.0 nm), which can fill up the supercages of MCM-22. However, there are few Pt particles larger than 2 nm observed in the sample.

Due to the beam sensitivity of zeolites, the location of the atoms/clusters cannot be investigated by focal-series studies[22,23]. However, the fact that we are performing these HAADF-HRSTEM studies in an aberration-corrected microscope offers the possibility to have access to the third dimension by varying the depth of focus. As can be seen in Supplementary Fig. 11, even if the structure of MCM-22 is destroyed (including mass loss) by the electron beam, Pt species still remain at the same position or move by just a few angstroms, indicating that these Pt atoms/clusters are probably embedded/anchored in the internal space of the zeolite crystallites. Nevertheless, information about the location of Pt species can be deduced according to the molecular sieving effect of MCM-22, which will be discussed in the section on catalytic activity.

The particle size distribution of subnanometric Pt species shown in Fig. 2i was obtained by counting more than 300 particles. A size

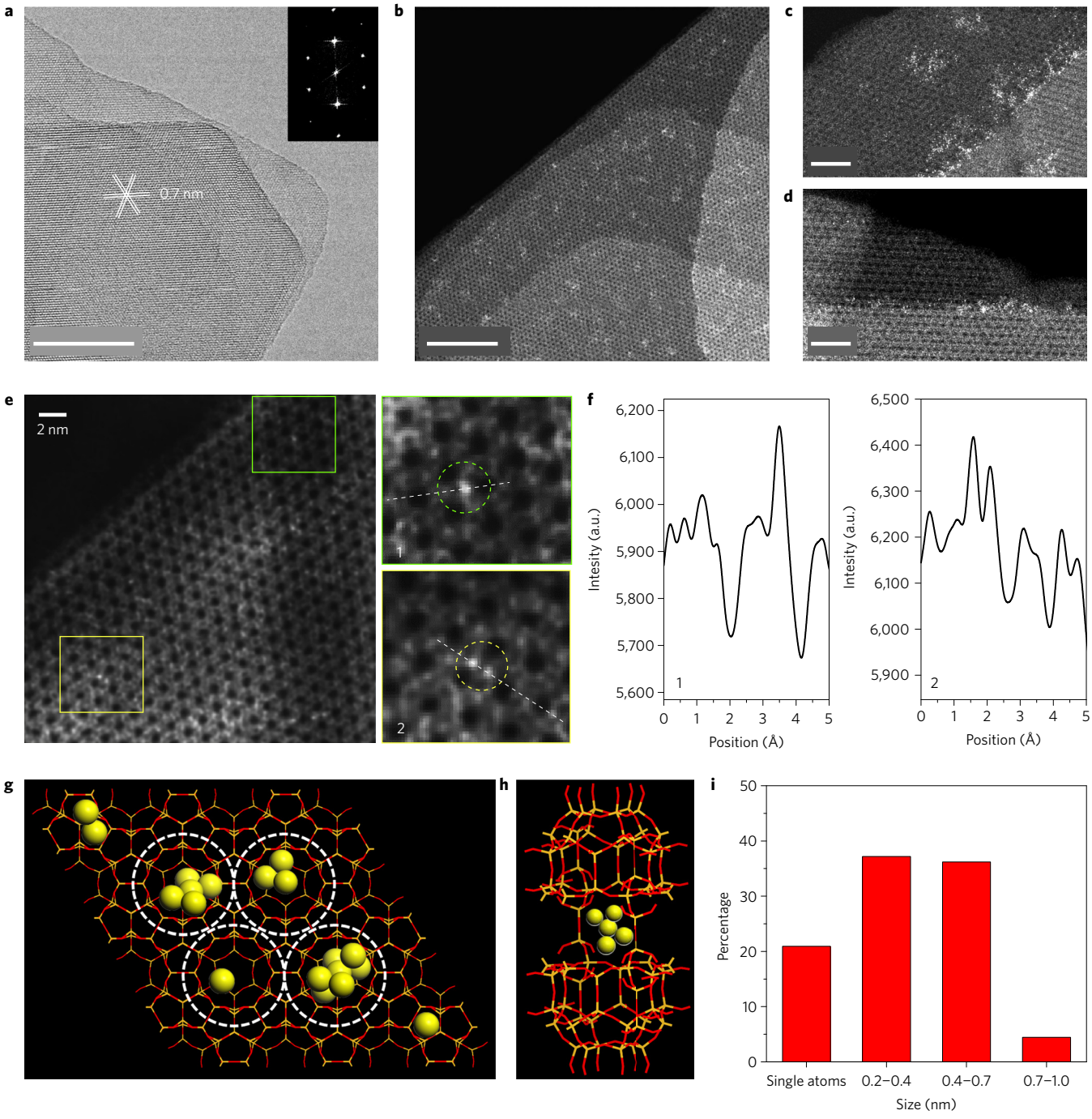

Figure 2 | Atomic structures of Pt@MCM-22. a, TEM image of Pt@MCM-22. The inset is the corresponding FFT diffractogram of the TEM image. Scale bar, 50 nm. **b**, HAADF-STEM image of Pt@MCM-22. Scale bar, 20 nm. **c**,**d**, Atomic structures of Pt clusters confined in MCM-22. Scale bar, 5 nm. **e**, HAADF-HRSTEM image of Pt@MCM-22, where two zoom-ins are shown in the square regions (marked in green (#1) and yellow (#2)). In these two areas, several single atoms have been highlighted. Scale bar, 2 nm. **f**, Corresponding intensity profiles obtained on the two zoomed areas in **e**. **g**, Schematic illustration of Pt@MCM-22 in a 'top-down' view along the *c* axis. Pt clusters and individual Pt atoms are located in the surface cups, cavities and 12-MR supercages. **h**, Schematic illustration of a Pt_5 cluster in supercages of MCM-22. **i**, Size distribution of subnanometric Pt species in a Pt@MCM-22 sample.

distribution ranging from single atoms to Pt clusters nearly to 1 nm in size, with a majority for Pt clusters between 0.2–0.7 nm, can be seen there. It has been reported that subnanometric metal species (single atoms and clusters) are unstable above 250 °C (refs 24–26). However, if one considers that the preparation procedure of Pt@MCM-22 includes a high-temperature process (540 °C for 4 h) for removal of the organic template, it appears that subnanometric Pt species in Pt@MCM-22 show excellent thermal stability in air.

Spectroscopic characterization of samples

A Pt@MCM-22 sample has been measured by X-ray adsorption spectroscopy (XAS) to study the local environment of Pt and to estimate the coordination numbers of Pt species. The Fourier transform of extended X-ray absorption fine structure (EXAFS) spectra of Pt@MCM-22 and the Pt and PtO_2 reference are shown in Fig. 3a and Supplementary Fig. 12. Considering the first shell, the Pt@MCM-22 spectrum is dominated by a peak centred around 2.65 Å with a smaller contribution at 2.08 Å (both distances not phase corrected).

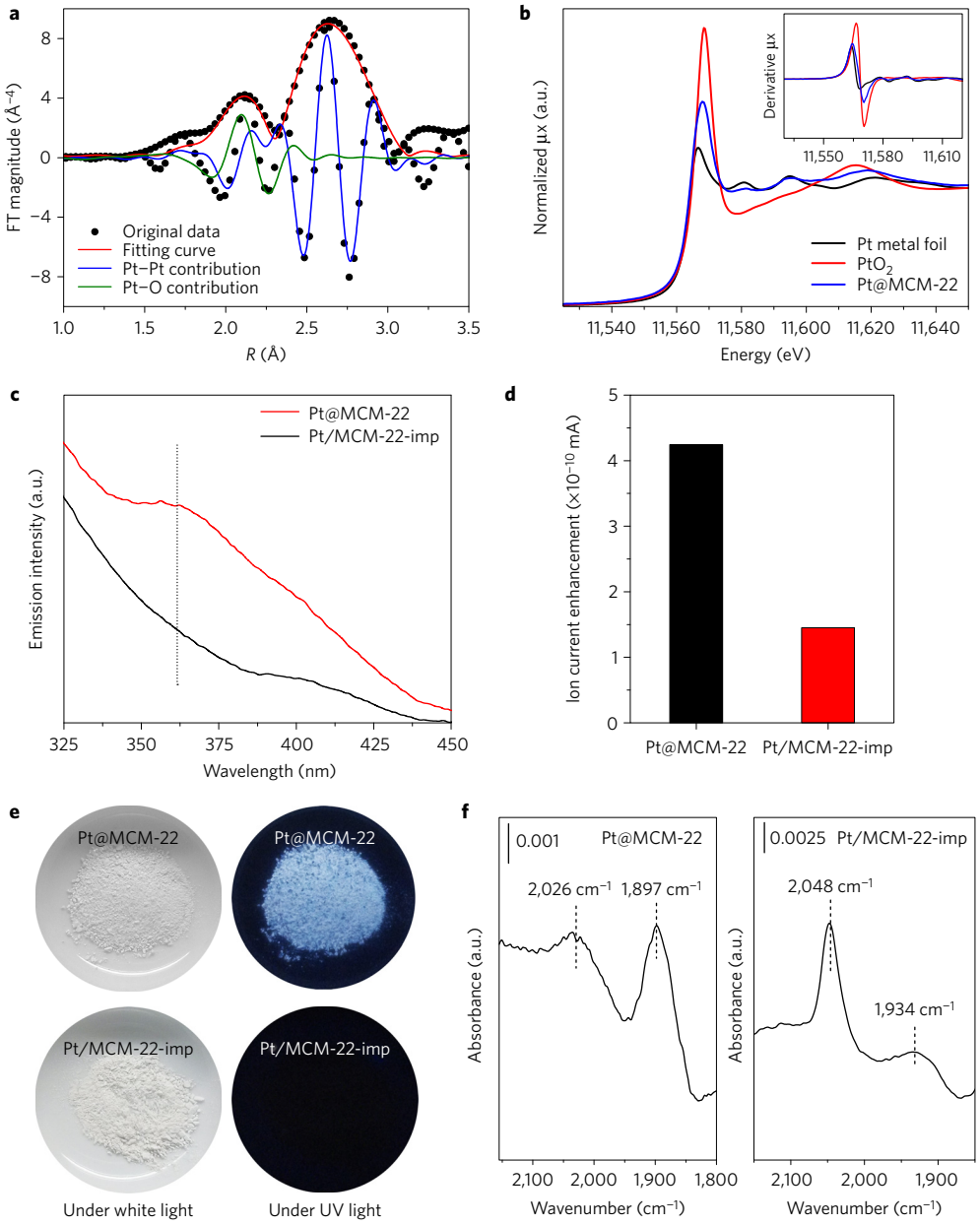

Figure 3 | Characterization of Pt@MCM-22 and Pt/MCM-22-imp. a, Fourier transform of k^3-weighted EXAFS spectrum of the Pt@MCM-22 sample (not phase corrected). The fitting curves for Pt–O and Pt–Pt contribution are also presented. **b**, XANES spectrum of Pt@MCM-22, with the first-order derivative spectrum given in the inset. **c**, Fluorescence emission spectra excited at 260 nm. **d**, Enhancement of the mass signal of HD in H_2–D_2 exchange experiments on Pt@MCM-22 and Pt/MCM-22-imp at room temperature. **e**, Photographs of Pt@MCM-22 and Pt/MCM-22-imp under white light and ultraviolet light. **f**, IR spectra of CO adsorption on Pt@MCM-22 and Pt/MCM-22-imp.

Comparing with reference samples, the stronger contribution can be assigned to Pt–Pt bonds in Pt clusters. The assignation of the weaker peak is too long to be ascribed to Pt–O bonds from PtO_2 (1.65 Å, see Supplementary Fig. 12), but according to literature data it is compatible with Pt–O bonds between Pt and the zeolite frameworks[27]. The presence of Pt–O bonds in Pt@MCM-22 sample has also been confirmed by the X-ray absorption near-edge structure (XANES) spectrum of Pt@MCM-22. As it can be seen in Fig. 3b, the curve shape of the Pt@MCM-22 sample looks like Pt(0) (first derivative and oscillations around 11,580 and 11,595 eV) but the white line intensity is higher, indicating the presence of Pt–O bonds[25]. Based on the fitting results of the EXAFS spectrum (see Table 1), the coordination number of Pt in Pt@MCM-22 is about 4.7, which would correspond to Pt clusters with a size of less than 0.7 nm (that is, with less than 13 atoms), assuming that Pt clusters show a cubo-octahedral shape[28,29]. Even though the atomicity of Pt species obtained based on EXAFS data is slightly larger than that obtained based on HRSTEM images, the average size is still in the cluster size range (below 0.7 nm), which is in line with the results obtained from electron microscopy and our synthesis principle.

As is well known, the optical properties of metal clusters and metal NPs are very different due to their distinct electronic structures. For comparison, we have prepared a Pt/MCM-22-imp sample with 0.2 wt% of Pt by a conventional impregnation method (see Methods). As shown in Supplementary Fig. 13, Pt NPs in the approximate size range of 1 to 5 nm are formed on MCM-22. The fluorescence emission spectra under excitation at 260 nm (see Fig. 3c) show that Pt@MCM-22 with Pt clusters presents a clear emission peak around 360 nm which can be associated with Pt clusters with fewer than 10 atoms[30,31]. In contrast, no fluorescence emission signal

Table 1 | Result of the fit performed on the Pt@MCM-22 EXAFS spectrum.

	CN	σ^2	R	E_0
Path		$Å^{-2}$	Å	eV
Pt-O	2.1 ± 0.6	0.004	2.506 ± 0.017	2.9
Pt-Pt	4.7 ± 0.5	0.005	2.765 ± 0.004	

$S_0^2 = 0.85$ fixed from the value extracted from the fit of the Pt foil, E_0 and σ^2 fixed from Pt foil; $\Delta k = (3.6\text{–}14.3)$ $Å^{-1}$ and $\Delta R = (1.4\text{–}3.5)$ Å. CN, coordination number; σ^2, Debye–Waller factor; R, distance; E_0, energy shift; S_0^2, many-body amplitude reduction factor. Δk and ΔR are the interval in the k space and in R space for the Fourier transform and the fitting, respectively.

can be observed in Pt/MCM-22-imp. The fluorescence emission of Pt clusters can also be seen from the pictures of the two samples under white light and ultraviolet light, respectively. As shown in Fig. 3e, strong fluorescent light emission can be observed in the Pt@MCM-22 sample under ultraviolet light.

To compare the different properties of subnanometric Pt species in Pt@MCM-22 and Pt NPs in Pt/MCM-22-imp on H_2 activation, H_2-D_2 exchange experiments were carried out[32]. Notice that H_2 can diffuse through the 8-MR window that communicates between the supercages in which a portion of the Pt species are encapsulated. The results given in Fig. 3d show that the formation rate of HD over Pt@MCM-22 is much higher than over Pt/MCM-22-imp, indicating that the subnanometric Pt species in Pt@MCM-22 are more active on the H_2 activation than the Pt NPs in Pt/MCM-22-imp, which is in agreement with the literature[33].

To investigate the chemical states of Pt species in Pt@MCM-22 and Pt/MCM-22-imp, CO was used as a probe molecule for IR spectroscopy. As shown in Fig. 3f, two CO adsorption bands can be observed, which can be ascribed to CO interacting in lineal and bridge configurations, respectively. The reported CO frequencies for Pt species in Pt@MCM-22 are lower than those observed for CO adsorbed in atop positions of Pt nanoparticles supported on MCM-22 and some conventional oxide carriers[34,35], which indicates a higher electron donor capacity of the subnanometric Pt species. It was suggested that the zeolite matrix can act as an electron donor, increasing the electron density of encapsulated Pt clusters[36]. On the other hand, small metal clusters may bear a higher electron charge due to their higher unsaturation degree, while specific supports could modify the net electronic charge of the clusters[37].

Catalytic activity

As has been presented above, incorporation of Pt in the expanded layered precursor of MCM-22 leads to isolated Pt atoms and Pt clusters on the cups located at the external surface and also probably in the internal space of MCM-22. On the other hand, in the case of the Pt/MCM-22-imp sample prepared by the impregnation method, most of Pt NPs ($1 \sim 5$ nm) should be located only at the external surface. To test the catalytic properties and to acquire more information on the location of Pt species in the Pt@MCM-22 sample, we have chosen hydrogenation of alkenes with different molecular sizes as probe reactions. First, the hydrogenation of propylene, which can diffuse through 8-MR windows and reach the supercavities with subnanometric Pt species, was performed in a fixed-bed reactor. Results in Fig. 4a show a higher activity of Pt@MCM-22 than Pt/MCM-22-imp. Notice that the reaction rate of Pt species is about five times higher for Pt@MCM-22. This difference of activity between Pt@MCM-22 and Pt/MCM-22-imp has also been observed before in the H_2-D_2 exchange experiment. The results would confirm the accessibility of propylene to all Pt species regardless of their location within the zeolite. However, as we said before, Pt species can also be encapsulated within 0.7×1.8 nm supercavities of MCM-22, which are accessible only through the 8-MR windows. As shown in Fig. 4b, the reaction rates for hydrogenation of isobutene

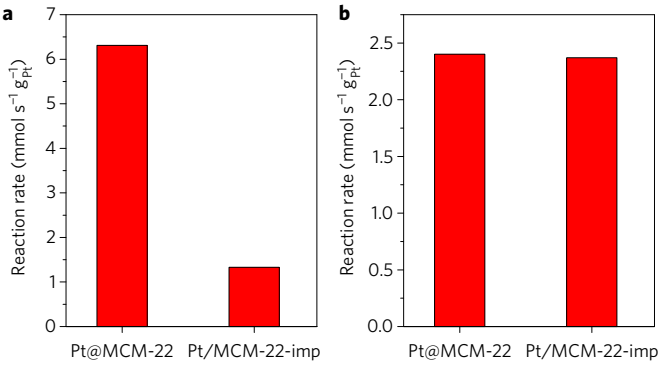

Figure 4 | Reaction rates of Pt@MCM-22 and Pt/MCM-22-imp in hydrogenation of light olefins. a,**b**, Hydrogenation of propylene (**a**) and hydrogenation of isobutene (**b**). The reaction rates are normalized based on the amount of Pt species in both catalysts.

of Pt/MCM-22-imp are similar to those of Pt@MCM-22, which is contrary to the activity difference for the propylene hydrogenation. Indeed, due to the molecular sieving effect of 8-MR windows in MCM-22, isobutene is accessible only to Pt species located at the external cups on the surface of MCM-22, while it should not be accessible to Pt atoms and clusters encapsulated in the cavities inside MCM-22. Therefore, by combining STEM characterization and the catalytic results on hydrogenation of propylene and isobutene, one can speculate that a large proportion of Pt species are located within the supercavities of MCM-22 in the Pt@MCM-22 sample.

High-temperature stability of Pt@MCM-22

The exceptional stability of the subnanometric Pt species in Pt@MCM-22 has been demonstrated by performing oxidation–reduction treatments at 650 °C. Under such harsh conditions, small Pt NPs with sizes of approximately 1 nm can be found in Pt@MCM-22 after one cycle of oxidation–reduction treatment at 650 °C (see Fig. 5a and Supplementary Fig. 14). Those individual Pt atoms and small Pt clusters with a few atoms located in the internal space of the MCM-22 crystallites have mostly aggregated to larger Pt clusters or small Pt NPs (in the range of 1 to 2 nm). As for Pt clusters with more than five atoms, they should be more stable because they are captured by the cups and supercages of MCM-22. Checking by STEM, we have observed some Pt clusters below 1 nm while few Pt individual atoms can be found on in the Pt@MCM-22-1cycle sample (as shown in Supplementary Fig. 15). With further cycles of oxidation–reduction treatments, Pt clusters will continue to grow larger, as presented in Fig. 5b–d (more STEM images can be found from Supplementary Figs 16–18). Nevertheless, their size distributions (Fig. 5f–h) show that most of the small Pt NPs are still below 2 nm, indicating the high stability of encapsulated Pt species in MCM-22 crystallites during the very extreme oxidation–reduction treatments at 650 °C. In the case of Pt/MCM-22-imp, oxidation–reduction treatments at 650 °C lead to continuous growth of Pt NPs (images are presented from Supplementary Figs 19 to 22 and the size distributions of Pt NPs are shown in Supplementary Fig. 23). In the Pt/MCM-22-imp-4cycles sample (Supplementary Fig. 22), some Pt NPs as large as $30 \sim 50$ nm are observed. However, it is important to take into account that, due to the lower melting and boiling point of Pt nanoclusters, subnanometric Pt species can be mobile during the high-temperature treatments, especially for those Pt species located on the external surface[38–40]. Thus, after four oxidation–reduction cycles at 650 °C, only ~30% of the initial Pt (measured by ICP) remain in the Pt@MCM-22 sample. Despite that, the stability against agglomeration of Pt species encapsulated in MCM-22 is still much better than the Pt/MCM-22-imp materials prepared through conventional impregnation methods.

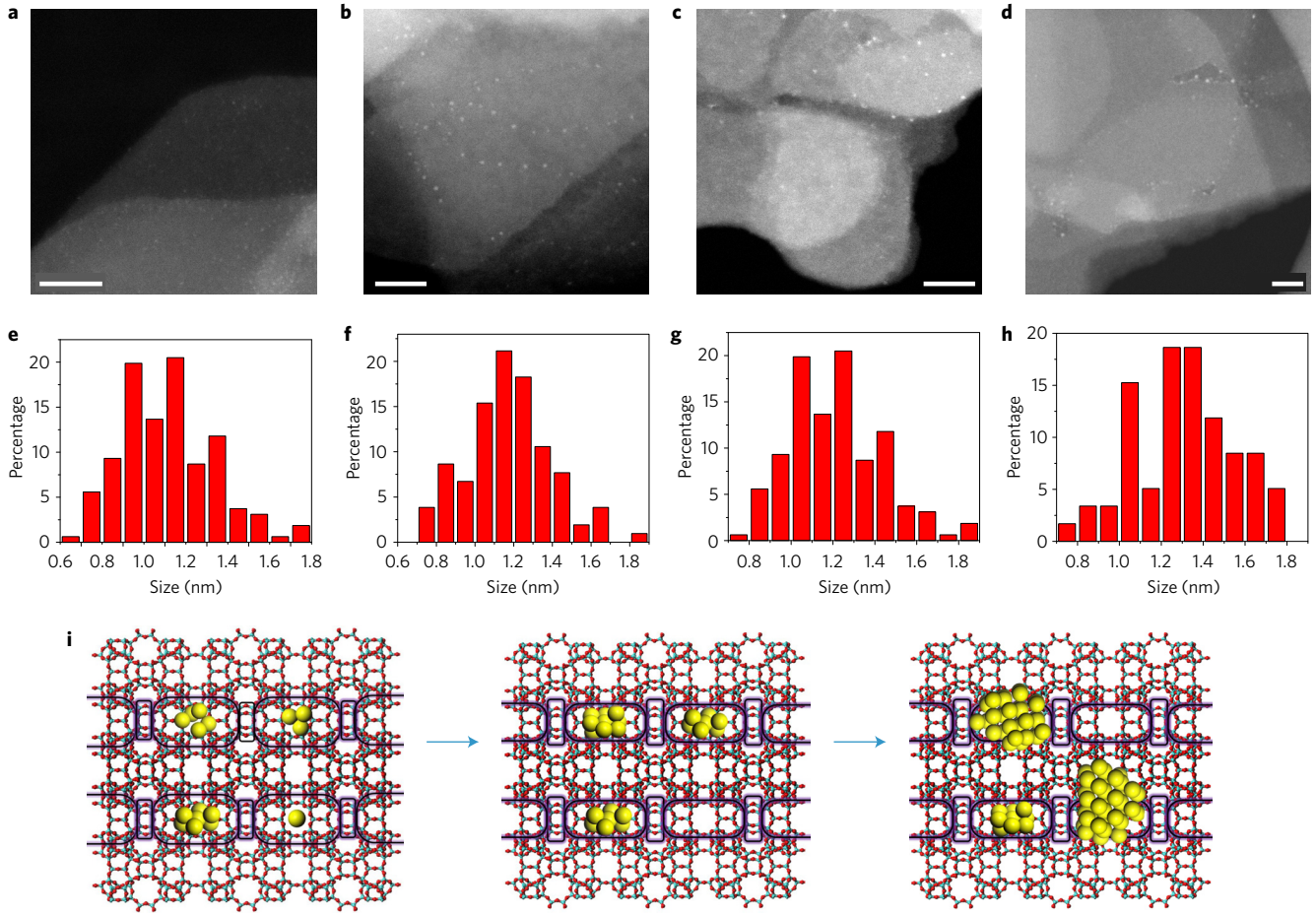

Figure 5 | Pt@MCM-22 after high-temperature oxidation–reduction treatments. a–d, STEM images of Pt@MCM-22 after different numbers of cycles of oxidation–reduction treatment at 650 °C. **a**, Pt@MCM-22-1cycle. **b**, Pt@MCM-22-2cycles. **c**, Pt@MCM-22-3cycles. **d**, Pt@MCM-22-4cycles. Scale bar in **a–d**, 20 nm. **e–h**, Size distributions of small Pt nanoparticles encapsulated in Pt@MCM-22 after different numbers of cycles of oxidation–reduction treatment at 650 °C. **e**, Pt@MCM-22-1cycle. **f**, Pt@MCM-22-2cycles. **g**, Pt@MCM-22-3cycles. **h**, Pt@MCM-22-4cycles. **i**, Schematic illustration of the evolution of individual Pt atoms and Pt clusters encapsulated in MCM-22 during the high-temperature oxidation–reduction treatments.

Taking into account the higher stability of Pt@MCM-22, we also decided to test its catalytic activity for dehydrogenation of propane. Indeed, dehydrogenation of short alkane molecules is of great interest to activate alkanes, and catalytic processes require frequent reaction–regeneration cycles at high temperature[41]. As can be seen in Supplementary Fig. 24, Pt@MCM-22 exhibits higher activity than Pt/MCM-22-imp at 550 °C. Moreover, after five reaction–regeneration cycles at 550 °C during the catalytic dehydrogenation of propane, Pt@MCM-22 sample retains ~90% of its initial activity while Pt/MCM-22-imp has lost more than 40% of its initial activity. It should be remarked that no significant loss of Pt in the Pt@MCM-22 sample is observed by ICP after five cycles of propane dehydrogenation reaction. In addition, the Pt@MCM-22 sample after two and five oxidation–reduction cycles at 550 °C has also been studied by STEM. As shown in Supplementary Figs 25 and 27, the particle sizes of most of the Pt species increase slightly, but still remain below 2 nm. Strong fluorescence emission under ultraviolet light can also be observed on those two samples (see Supplementary Fig. 27), indicating the presence of Pt clusters even after treatments at 550 °C. This is in agreement with the higher thermal stability of the Pt@MCM-22 sample.

Conclusions

We have presented a new strategy to prepare subnanometric Pt catalysts in 3D MCM-22 zeolite with exceptional high stability, starting from 2D MWW-type precursors. Pt single atoms and clusters are stable after calcination in air at 540 °C and under reaction conditions. This new method provides a possibility for the generation of highly stable subnanometric metal catalysts for high-temperature catalytic reactions in pure siliceous zeolites.

Methods

Methods and any associated references are available in the online version of the paper.

Received 4 December 2015; accepted 18 August 2016; published online 26 September 2016

References

1. Boronat, M., Leyva-Perez, A. & Corma, A. Theoretical and experimental insights into the origin of the catalytic activity of subnanometric gold clusters: attempts to predict reactivity with clusters and nanoparticles of gold. *Acc. Chem. Res.* **47,** 834–844 (2014).
2. Flytzani-Stephanopoulos, M. & Gates, B. C. Atomically dispersed supported metal catalysts. *Ann. Rev. Chem. Bio. Eng.* **3,** 545–574 (2012).
3. Gates, B. C. Supported metal clusters: synthesis, structure, and catalysis. *Chem. Rev.* **95,** 511–522 (1995).
4. Corma, A. *et al*. Exceptional oxidation activity with size-controlled supported gold clusters of low atomicity. *Nat. Chem.* **5,** 775–781 (2013).
5. Yang, M. *et al*. Catalytically active Au-O(OH)$_x$-species stabilized by alkali ions on zeolites and mesoporous oxides. *Science* **346,** 1498–1501 (2014).
6. Rivallan, M. *et al*. Platinum sintering on H-ZSM-5 followed by chemometrics of CO adsorption and 2D pressure-jump IR spectroscopy of adsorbed species. *Angew. Chem. Int. Ed.* **49,** 785–789 (2010).

7. Zecevic, J., van der Eerden, A. M., Friedrich, H., de Jongh, P. E. & de Jong, K. P. Heterogeneities of the nanostructure of platinum/zeolite Y catalysts revealed by electron tomography. *ACS Nano* **7,** 3698–3705 (2013).
8. Philippaerts, A. *et al*. Unprecedented shape selectivity in hydrogenation of triacylglycerol molecules with Pt/ZSM-5 zeolite. *Angew. Chem. Int. Ed.* **50,** 3947–3949 (2011).
9. Kim, J., Kim, W., Seo, Y., Kim, J.-C. & Ryoo, R. n-Heptane hydroisomerization over Pt/MFI zeolite nanosheets: effects of zeolite crystal thickness and platinum location. *J. Catalys.* **301,** 187–197 (2013).
10. Goel, S., Wu, Z., Zones, S. I. & Iglesia, E. Synthesis and catalytic properties of metal clusters encapsulated within small-pore (SOD, GIS, ANA) zeolites. *J. Am. Chem. Soc.* **134,** 17688–17695 (2012).
11. Choi, M., Wu, Z. & Iglesia, E. Mercaptosilane-assisted synthesis of metal clusters within zeolites and catalytic consequences of encapsulation. *J. Am. Chem. Soc.* **132,** 9129–9137 (2010).
12. Choi, M., Yook, S. & Kim, H. Hydrogen spillover in encapsulated metal catalysts: new opportunities for designing advanced hydroprocessing catalysts. *ChemCatChem* **7,** 1048–1057 (2015).
13. Kulkarni, A., Lobo-Lapidus, R. J. & Gates, B. C. Metal clusters on supports: synthesis, structure, reactivity, and catalytic properties. *Chem. Commun.* **46,** 5997–6015 (2010).
14. Guzman, J. & Gates, B. C. Supported molecular catalysts: metal complexes and clusters on oxides and zeolites. *Dalton Trans.* **1,** 3303–3318 (2003).
15. Leonowicz, M. E., Lawton, J. A., Lawton, S. L. & Rubin, M. K. MCM-22: a molecular sieve with two independent multidimensional channel systems. *Science* **264,** 1910–1913 (1994).
16. Camblor, M. A. *et al*. A new microporous polymorph of silica isomorphous to zeolite MCM-22. *Chem. Mater.* **8,** 2415–2417 (1996).
17. Hyotanishi, M., Isomura, Y., Yamamoto, H., Kawasaki, H. & Obora, Y. Surfactant-free synthesis of palladium nanoclusters for their use in catalytic cross-coupling reactions. *Chem. Commun.* **47,** 5750–5752 (2011).
18. Duchesne, P. N. & Zhang, P. Local structure of fluorescent platinum nanoclusters. *Nanoscale* **4,** 4199–4205 (2012).
19. Lu, J., Aydin, C., Browning, N. D. & Gates, B. C. Imaging isolated gold atom catalytic sites in zeolite NaY. *Angew. Chem. Int. Ed.* **51,** 5842–5846 (2012).
20. Yacamán, M. J., Santiago, U. & Mejía-Rosales, S. in *Advanced Transmission Electron Microscopy: Applications to Nanomaterials* (eds Francis, L., Mayoral, A. & Arenal, R.) 1–29 (Springer, 2015).
21. Jena, P., Khanna, S. N. & Rao, B. K. *Physics and Chemistry of Finite Systems: From Clusters to Crystals* (Springer, 1992).
22. Yamasaki, J. *et al*. *Ultramicroscopy* **151,** 224–231 (2015).
23. Sohlberg, K., Pennycook, T. J., Zhoud, W. & Pennycook, S. J. Insights into the physical chemistry of materials from advances in HAADF-STEM. *Phys. Chem. Chem. Phys.* **17,** 3982–4006 (2015).
24. Aydin, C., Lu, J., Browning, N. D. & Gates, B. C. A 'smart' catalyst: sinter-resistant supported iridium clusters visualized with electron microscopy. *Angew. Chem. Int. Ed.* **51,** 5929–5934 (2012).
25. Wei, H. *et al*. FeO_x-supported platinum single-atom and pseudo-single-atom catalysts for chemoselective hydrogenation of functionalized nitroarenes. *Nat. Commun.* **5,** 5634 (2014).
26. Addou, R. *et al*. Influence of hydroxyls on Pd atom mobility and clustering on rutile $TiO_2(011)$-2 × 1. *ACS Nano* **8,** 6321–6333 (2014).
27. Jung, U. *et al*. Comparative in operando studies in heterogeneous catalysis: atomic and electronic structural features in the hydrogenation of ethylene over supported Pd and Pt catalysts. *ACS Catal.* **5,** 1539–1551 (2015).
28. Agostini, G. *et al*. Effect of different face centered cubic nanoparticle distributions on particle size and surface area determination: a theoretical study. *J. Phys. Chem. C* **118,** 4085–4094 (2014).
29. Alexeev, O. & Gates, B. C. EXAFS characterization of supported metal-complex and metal-cluster catalysts made from organometallic precursors. *Top. Catal.* **10,** 273–293 (2000).
30. Chakraborty, I., Bhuin, R. G., Bhat, S. & Pradeep, T. Blue emitting undecaplatinum clusters. *Nanoscale* **6,** 8561–8564 (2014).
31. Zheng, J., Nicovich, P. R. & Dickson, R. M. Highly fluorescent noble-metal quantum dots. *Ann. Rev. Phys. Chem.* **58,** 409–431 (2007).
32. Okrut, A. *et al*. Selective molecular recognition by nanoscale environments in a supported iridium cluster catalyst. *Nat. Nanotech.* **9,** 459–465 (2014).
33. Zhou, C. *et al*. On the sequential hydrogen dissociative chemisorption on small platinum clusters: a density functional theory study. *J. Phys. Chem. C* **111,** 12773–12778 (2007).
34. De La Cruz, C. & Sheppard, N. An exploration of the surfaces of some Pt/SiO_2 catalysts using CO as an infrared spectroscopic probe. *Spectrochim. Acta A* **50,** 271–285 (1994).
35. Klünker, C., Balden, M., Lehwald, S. & Daum, W. CO stretching vibrations on Pt(111) and Pt(110) studied by sum frequency generation. *Surf. Sci.* **360,** 104–111 (1996).
36. Stakheev, A. Y., Shpiro, E. S., Jaeger, N. I. & Schulz-Ekloff, G. Electronic state and location of Pt metal clusters in KL zeolite: FTIR study of CO chemisorption. *Catal. Lett.* **32,** 147–158 (1995).
37. Heiz, U., Sanchez, A., Abbet, S. & Schneider, W. D. Catalytic oxidation of carbon monoxide on monodispersed platinum clusters: each atom counts. *J. Am. Chem. Soc.* **121,** 3214–3217 (1999).
38. Levitas, V. I. & Samani, K. Size and mechanics effects in surface-induced melting of nanoparticles. *Nat. Commun.* **2,** 284 (2011).
39. Jiang, H., Moon, K.-s., Dong, H., Hua, F. & Wong, C. P. Size-dependent melting properties of tin nanoparticles. *Chem. Phys. Lett.* **429,** 492–496 (2006).
40. Nanda, K. K., Kruis, F. E. & Fissan, H. Evaporation of free PbS nanoparticles: evidence of the Kelvin effect. *Phys. Rev. Lett.* **89,** 256103 (2002).
41. Vajda, S. *et al*. Subnanometre platinum clusters as highly active and selective catalysts for the oxidative dehydrogenation of propane. *Nat. Mater.* **8,** 213–216 (2009).

Acknowledgements

This work was funded by the Spanish Government (Consolider Ingenio 2010-MULTICAT (CSD2009-00050) and MAT2014-52085-C2-1-P) and by the Generalitat Valenciana (Prometeo). The Severo Ochoa Program (SEV-2012-0267) is gratefully acknowledged. L.L. thanks ITQ for a contract. The authors also thank the Microscopy Service of UPV for the TEM and STEM measurements. The HAADF-HRSTEM works were conducted in the Laboratorio de Microscopias Avanzadas (LMA) at the Instituto de Nanociencia de Aragon (INA)-Universidad de Zaragoza (Spain), a Spanish ICTS National Facility. Some of the research leading to these results has received funding from the European Union Seventh Framework Program under Grant Agreement 312483-ESTEEM2 (Integrated Infrastructure Initiative-I3). R.A. also acknowledges funding from the Spanish Ministerio de Economia y Competitividad (FIS2013-46159-C3-3-P) and the European Union Horizon 2020 research and innovation programme under the Marie Sklodowska-Curie grant agreement No. 642742.

Author contributions

A.C. conceived the project, directed the study and wrote the manuscript. L.L. carried out the synthesis, characterization and catalytic measurements and collaborated in writing the manuscript. U.D. participated in the synthesis and characterization of the materials. R.A. performed the high-resolution STEM characterization. G.A. performed the XAS measurement and analysed the data. P.C. carried out the H_2–D_2 exchange and CO-IR adsorption experiments. U.D., R.A., G.A. and P.C. also collaborated in writing the manuscript.

Additional information

Supplementary information is available in the online version of the paper. Reprints and permissions information is available online at www.nature.com/reprints. Correspondence and requests for materials should be addressed to A.C.

Competing financial interests

The authors declare no competing financial interests.

Methods

Synthesis of the solution containing Pt clusters. Subnanometric Pt species were prepared by a dimethylformamide (DMF) reduction method. 20 mg $Pt(acac)_2$ (Platinum(II) acetylacetonate) were dissolved in 40 ml DMF. Then the solution was heated at 140 °C for 16 h. After the heating process, the excess DMF in the solution was removed with a rotary evaporator, resulting in a Pt-DMF solution of around 10 ml.

Synthesis of ITQ-1 and Swelled ITQ-1. ITQ-1 zeolite (IZA code MWW) is the pure-silica analogue of MCM-22. It could be synthesized using trimethyladamantammonium ($TMAda^+$) as a structure-directing agent in the absence of alkali cations, but reproducibility problems appeared. If hexamethyleneimine (HMI) is added as second SDA, the reproducibility of the synthesis, as well as the quality of the materials obtained, are greatly improved. The use of $TMAda^+$, HMI and sodium cations allows a fast and highly reproducible synthesis of pure-silica ITQ-1.

An example of the procedure for the synthesis of ITQ-1 using $TMAda^+$, HMI and Na^+ cations is as follows: 0.95 g of NaCl was dissolved in 50.70 g of a solution 0.42 M of *N,N,N*-trimethyl-1-adamantanamonium hydroxide, previously diluted with 21.33 g of water. Then, 2.62 g of hexamethyleneimine was added to this solution, followed by 4.88 g of silica (Aerosil 200, Degussa) under continuous stirring. This reaction mixture was heated in a PTFE-lined stainless steel autoclave at 150 °C rotated at 60 r.p.m. for five days. After filtering, the white solid obtained was washed until the pH was less than 9.

To prepare the swelled purely siliceous ITQ-1 with subnanometric Pt species, 2 g of the lamellar precursor was dispersed in 8 g of H_2O milliQ, and 40 g of a cetyltrimethylammonium hydroxide solution (25 wt%, 50% exchanged Br^-/OH^-) and 12 g of a solution of tetrapropylammonium hydroxide (40 wt%, 30% exchanged Br^-/OH^-) were added together with 40 ml of Pt-DMF solution, the final pH being around 12.5. The resultant mixture was heated at 52 °C, stirring vigorously, for 16 h to facilitate the swelling of the layers of the precursor material. At this point, the solid was recovered by centrifugation and washed with distilled water, and then dried at 60 °C for 12 h.

Synthesis of Pt@MCM-22. Pt@MCM-22 can be obtained through the calcination of the Pt@Swelled MWW(P) composite. The calcination process was performed as follows. First, the temperature was raised from room temperature to 540 °C at a ramp rate of 2 °C min^{-1} in a N_2 atmosphere. The total time in the N_2 atmosphere was about 4.5 h. Next, the atmosphere was switched from N_2 to air and maintained at a temperature of 540 °C for 4 h. Finally, in the cooling phase, the temperature was reduced from 540 °C to room temperature in an air atmosphere. The obtained sample is denoted as Pt@MCM-22.

Stability test of Pt@MCM-22 samples. To test the thermal stability of the subnanometric Pt species, a high-temperature oxidation–reduction cyclic treatment was used. Fresh Pt@MCM-22 sample was first subjected to an oxidation treatment at 650 °C in air (temperature ramp rate 2 °C min^{-1} and maintained at 650 °C for 2 h). After the oxidation treatment, the sample was reduced at 650 °C in H_2 (temperature ramp rate 2 °C min^{-1} and maintained at 650 °C for 2 h). The above reduction and oxidation treatment were considered as one cycle and the sample after one-cycle treatment is called Pt@MCM-22-1cycle. In a similar way, the Pt@MCM-22-1cycle can be further applied in consecutive oxidation–reduction cycles.

Preparation of Pt/MCM-22-imp through impregnation method. To compare with the Pt@MCM-22 materials, the Pt/MCM-22-imp sample was prepared through a conventional wet-impregnation method. MCM-22 (prepared through the calcination of ITQ-1) was used as the support. DMF solution containing subnanometric Pt species was used as the precursor for Pt nanoparticles. In a typical preparation of Pt/MCM-22-imp with 0.2 wt% of Pt, 2.2 g MCM-22 (pure silica) was firstly dispersed in 25 ml of H_2O and 35 ml of Pt-DMF solution. The suspension was kept stirring at room temperature for 30 min and then sent to a silicone oil bath at 120 °C to remove the solvent. After removing the solvent, the solid was dried in air at 100 °C for 16 h. Finally, Pt/MCM-22-imp can be obtained after reduction in H_2 at 450 °C (temperature ramp rate 5 °C min^{-1}) for 3 h.

We have also tried to use the incipient wetness impregnation (IWI) method to prepare supported Pt nanoparticles on MCM-22. However, the dispersion of Pt obtained by the IWI method does not give a better dispersion of Pt species on MCM-22.

Characterization. Samples for electron microscopy studies were prepared by dropping the suspension of Pt@MCM-22 or other materials, using ethanol as the solvent, directly onto holey-carbon-coated Cu grids. The measurements were performed using a JEOL 2100F microscope operating at 200 kV, both in transmission (TEM) and scanning-transmission modes (STEM). STEM images were obtained using a high-angle annular dark-field detector (HAADF), which allows Z-contrast imaging. The current density is 0.9 pA cm^{-2} when working on the JEOL 2100F. High-resolution STEM (HRSTEM) imaging, using the HAADF detector, was performed using a FEI Titan Low-Base microscope operated at 300 kV and equipped with a Cs probe corrector (CESCOR from CEOS GmbH), a monochromator and an ultra-bright X-FEG electron source. The convergence angle was 25 mrad and the inner and outer angles for HAADF imaging were 70 and 200 mrad, respectively. The typical probe current was set to 2 pA and the total dose on the sample varied between ~0.2–3 C cm^{-2} under the HRSTEM imaging conditions, which corresponds to low-dose conditions[42]. Multi-slice HAADF-HRSTEM image simulations have been carried out using QSTEM software[43], with the experimental settings of the FEI Titan Low Base as inputs. For this purpose, the thermal diffuse scattering parameter was fixed at 30 for a temperature of 300 K.

Hydrogen/deuterium (H_2-D_2) exchange experiments were carried out in a flow reactor at room temperature (25 °C). The formation rate of HD species can be measured by the enhancement of the mass signal intensity (ion current). The feed gas consisted of 4 ml min^{-1} H_2, 4 ml min^{-1} D_2 and 18 ml min^{-1} argon, and the total weight of catalyst was 115 mg. The sample has been diluted with 230 mg of SiC. Reaction products (H_2, HD and D_2) were analysed with a mass spectrometer (Omnistar, Balzers). The m/z mass values used are 2 for H_2, 4 for D_2 and 3 for HD. The sample was *in situ* reduced at 200 °C for 2 h with a temperature-ramp rate of 10 °C/min from room temperature to 200 °C. Then the temperature was decreased to 25 °C and, once stabilized, the H_2 feed was changed to the reactant gas composition. The temperature was maintained at 25 °C for about 60 min.

Powder X-ray diffraction (XRD) was performed with a HTPhilips X'Pert MPD diffractometer equipped with a PW3050 goniometer using Cu Kα radiation and a multisampling handler.

XAS measurements were carried out on the BM23 beamline at the ESRF facility (Grenoble, France). Fluorescence XAS spectra at the Pt L_3-edge (11.564 keV) were collected with a 13-element Ge detector on a self-supported pellet at room temperature. A Pt reference foil was collected for energy calibration. The beam energy were selected by a double-crystal Si(111) monochromator, with third-harmonic rejection performed by means of a Rh-coated mirror at an angle of −4 mrad (ref. 44). EXAFS signals were extracted and analysed using the IFEFFIT package[45].

Measurement of catalytic performance of Pt@MCM-22 and Pt/MCM-22-imp. Hydrogenation of propylene was performed in a flow fixed-bed continuous reactor. 30 mg Pt@MCM-22 diluted with 2 g SiC (the grain size of SiC used in this work is between 0.4 to 0.6 mm) powder was loaded in a quartz tube reactor. The reaction was performed at room temperature with a flow of 2 ml min^{-1} of propylene, 6 ml min^{-1} of H_2 and 32.7 ml min^{-1} of Ar. Products were analysed with a Bruker on-line gas chromatograph (GC) with flame ionization detector (FID). The conversion of C_3H_6 was kept below 15% to calculate the reaction rates.

Hydrogenation of isobutene was performed in a flow fixed-bed continuous reactor. 30 mg Pt@MCM-22 diluted with 2 g SiC powder was loaded in a quartz tube reactor. The reaction was performed at room temperature with a flow of 1.5 ml min^{-1} of isobutene, 4.5 ml min^{-1} of H_2 and 24 ml min^{-1} of Ar. Products were analysed by a Bruker on-line GC with FID detector. The conversion of isobutene was kept below 15% when the calculating reaction rates.

Dehydrogenation of propane was performed in a fixed-bed reactor. A cylindrical quartz tube was loaded with 1.10 g of Pt@MCM-22 catalyst material (in the case of Pt/MCM-22-imp, the amount of catalyst was 0.60 g). Catalyst was diluted with SiC to keep the total volume of solid constant (3 cm^3). Before the reaction, the sample was reduced by H_2 at 550 °C. The reaction was run at 550 °C with a flow of 30 ml min^{-1} of propane and 3 ml min^{-1} of N_2 for 15 min, followed by a regeneration step at 550 °C with a flow of air for 30 min. The reaction stream was analysed by an on-line Varian GC, which was equipped with a flame ionization detector (FID) and a thermal conductivity detector (TCD). Conversion of C_3H_8 was kept below 10% to calculate the initial reaction rate.

References

42. Ortalan, V., Uzun, A., Gates, B. C. & Browning, N. D. Direct imaging of single metal atoms and clusters in the pores of dealuminated HY zeolite. *Nat. Nanotech.* **5,** 506–510 (2010).
43. Koch, C. *Determination of Core Structure Periodicity and Point Defect Density along Dislocations* PhD thesis, Univ. Arizona (2002).
44. Mathon, O. *et al*. The time-resolved and extreme conditions XAS (TEXAS) facility at the European Synchrotron Radiation Facility: the general-purpose EXAFS bending-magnet beamline BM23. *J. Synchrotron Radiat.* **22,** 1548–1554 (2015).
45. Newville, M. IFEFFIT: interactive XAFS analysis and FEFF fitting. *J. Synchrotron Radiat.* **8,** 322–324 (2001).